# Supporting information

## Field-Scale Heterogeneity and Geochemical Regulation of Arsenic, Iron, Lead, and Sulphur Bioavailability in Paddy Soil

Wen Fang[†], Paul N. Williams[§*], Xu Fang[†¥], Collins Amoah-Antwi[§], Daixia Yin[†], Gang Li[⊥], Lena Q. Ma[†], Jun Luo[†*]

[†] State Key Laboratory of Pollution Control and Resource Reuse, School of the Environment, Nanjing University, Nanjing, Jiangsu 210023, China

[¥]Institute of Biogeochemistry and Pollutant Dynamics, Department of Environmental Systems Science. ETH zurich , 8092 Zürich. Switzerland.

[§]Institute for Global Food Security, Queen's University Belfast, David Keir Building, Malone Road, Belfast, BT9 5BN, Northern Ireland.

[⊥]Key Laboratory of Urban Environment and Health, Institute of Urban Environment, Chinese Academy of Sciences, Xiamen, China.

Number of pages: 25

Number of figures: 9

Number of tables: 8

TABLE OF CONTENTS

**A summary of the methodology for high-resolution 2D imaging of the rice soil environment using DGT probe**

A DGT probe with the traditional dimension was deployed in a paddy field near the rice root after deoxygenated for at least 12 hrs in 0.01 mol $L^{-1}$ $NaNO_3$ via sparging with $N_2$ gas. The DGT probe was gently pushed into the paddy soil, to approximately the level of the soil-water interface (SWI). After deployment for 24 hrs, the probe was retrieved from the field for measurement. The probe was jet-washed with Milli-Q (MQ) water and wiped clean with laboratory-grade tissue paper prior to being placed in zip-lock clean bags for transfer back to the laboratory for disassembling.

Preparation of DGT gel for LA-ICP-MS analysis was carried out according to Gao and Lehto (2012) [1]. DGT gels were placed on an acid-washed 0.45-μm cellulose nitrate filter with a backing layer of laboratory-grade tissue paper. Gels were air dried overnight and subsequently dried in a gel dryer (Model 583, Biorad, Hercules, CA) at 60ºC for 8 hours prior to LA-ICP-MS analysis. The dried DGT gel was laser ablated by a Nd:YAG solid-state laser ablation system (New Wave, Cambridge, U.K.), then transported in the form of aerosols via helium carrier gas to the ICP-MS (Thermo X series 2) for elemental analysis. The laser was set-up first with primary calibrations on National Institute of Standards and Technology (NIST) glass standard 612. The LA-ICP-MS system was optimized, principally by adjusting gas flow rates, torch sampling depth, and RF power to achieve the maximum signal intensity and stability of target elements while minimizing interferences. Carbon (m/z 13) was used as an internal standard to cancel out variations in ablation, transport, and ionization efficiency.

[1] Gao, Y.; Lehto, N. A simple laser ablation ICP-MS method for the determination of trace metals in a resin gel. *Talanta*. **2012**, *92*, 78-83.

**Standard Calibrations for DGT Gels.**

Conventional DGT device moldings were obtained from the DGT Research® (Lancaster, UK). Together with all the PADDI probes, they were acid washed (10% $HNO_3$) and rinsed with MQ water prior to use. Arsenic calibrations for PF and PZ gels were made by deploying PF-DGT and PZ-DGT devices in a 0.01 M $NaNO_3$ solution prepared with MQ water, containing 100−800 μg $L^{-1}$ As ($Na_3AsO_4$) for 4 hrs. Lead and Fe calibrations for SPR-IDA gel were made by deploying SPR-IDA DGT devices in standard solutions with concentrations of 20−160 μg $L^{-1}$ of Pb ($PbNO_3$) for 4 hrs and 2−10 mg $L^{-1}$ of Fe ($FeSO_4$) for 10−33 hrs, respectively. All deployments were carried out in controlled temperature (24 $^{o}$C) and pH environments. For Pb and As standard solutions, pH was monitored to be within 5.0−6.5 throughout the experiments. The Fe calibration deployments were performed under anoxic conditions at a pH of 5.5 to avoid the oxidation and precipitation of Fe(III).

All the DGT devices deployed for the calibration standards were replicated (n = 3). Mass loadings of Pb and As on DGT gels were calculated directly from their measured concentrations in standard solutions before and after DGT device deployment. For Fe, the mass loading on the gel was determined by eluting one replicate of SPR-IDA gel with 1M $HNO_3$ and then measuring the concentration in the elution by flame atomic absorption spectrophotometry (FAAS; PinAAcle 900T, PerkinElmer).

Element concentrations for Pb, As and Fe, in the standard gels were also determined by LA-ICPMS. The relationship between the mass loading of the gels (ng $cm^{-2}$) and the normalized metal count rate (metal count rate divided by $^{13}$C-count rate) were plotted as linear standard calibrations (***Figure S3***).

**Description of soil sampling for field characterization**

Soil samples were collected at the depth about 15 cm in each site in July, 2016 to evaluate the horizontal distribution. Then two soil core samples with depth of 25 cm were collected in site 7 and 8 in September, 2016 and soil core samples were sliced into ~5 cm long sections investigate the vertical distribution. All the soil samples were air-dried for the following physicochemical properties analysis.

**Determination of pH, TOC, porosity, and total contents of As, Fe, and Pb in soils**

The pH was determined by extraction of the samples with 0.01M $CaCl_2$ at a liquid to solid ratio (L/S) of 5 L/kg. 5 g samples and 25 mL 0.01M $CaCl_2$ were added to the bottle, which was then tumbled for 1 h at the 150 rpm at the room temperature. After that, the pH of the supernatant was measured.

TOC in the solid matrix was determined by the high-temperature combustion method with a Shimadzu solid sample module coupled to a TOC analyzer (TOC-cvph: Shimadzu, Kyoto, Japan). Two separate furnaces, one for TC, was set at 900 °C and the other for TIC was set at 200 °C. The content of TOC was calculated by subtracting TIC from TC.

Soil porosity (ϕ) within the core samples was calculated according to ***Eq. S1*** by assuming that soil was saturated with water and density of soil particle was 2.65 $g/cm^3$ [1].

$$\phi = \frac{M_{wet} - M_{dry}}{M_{wet} - M_{dry} + \frac{M_{dry}}{2.65}} \quad \textbf{(S1)}$$

Total contents of heavy metals in soils were determined after acid digestion based on the EPA Method 3050B. After digestion and filtration, total contents of metals (As, Pb, and Fe) in soils were determined by inductively coupled plasma mass spectrometry (ICP-MS) (NexION300X, PerkinElmer) and flame atomic absorption spectrophotometry (FAAS) (PinAAcle 900T, PerkinElmer).

[1] Bielders, C. L., De Backer, L. W., & Delvaux, B. Particle density of volcanic soils as measured with a gas pycnometer. *Soil Science Society of America Journal*. 1990, *54*(3), 822-826.

**Relevant information on DGT theory and its principal to determine the bioavailable concentration of elements**

Diffusive gradients in thin films (DGT) is a passive sampling technique which is based on Fick's first law of diffusion. Analytes diffuse through the well-defined diffusive layer and filter membrane and immediately bind to a binding layer, which results in an effective zero concentration at the diffusive and binding layer interface, forming a linear steady state concentration gradients.

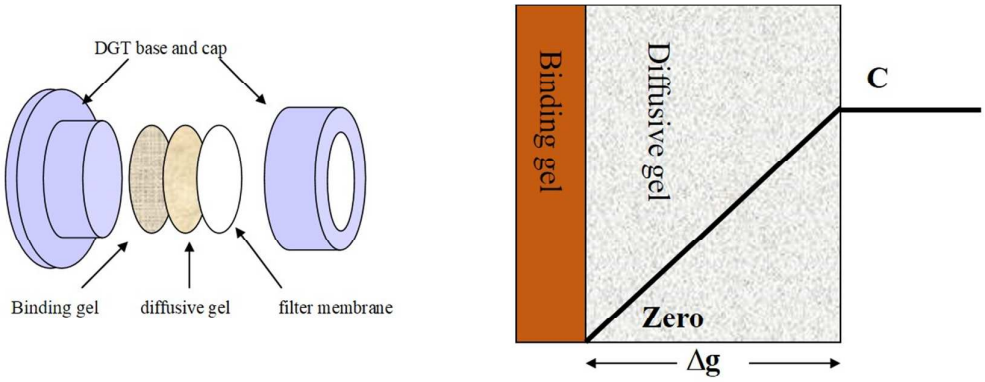


**Figure S1.** The components of DGT device and its principal to measure labile concentration

According to Fick's first law, the flux (F) of an analyte through the diffusive gel and filter can be expressed as (***Eq. S2***).

$$\mathrm{F} = D\frac{\partial C}{\partial x} = D\frac{(\mathrm{C}-\mathrm{C}')}{\Delta g} \qquad \textbf{(S2)}$$

Where D is the diffusion coefficient of an analyte in the diffusive gel and filter membrane, ∂C/∂x is the concentration gradient, C is the analyte concentration in the solution, C', the concentration of the analyte at the interface of binding layer and diffusive layer, and Δg is the thickness of the diffusive gel and filter membrane. Before the binding layer reaches saturated, C' equals to zero. Then ***Eq. S3*** becomes ***Eq. S4***.

$$\mathrm{F} = D\frac{C}{\Delta g} \qquad \textbf{(S3)}$$

Flux, F, can also be expressed as ***Eq. S4***.

$$F = \frac{M}{At} \quad \textbf{(S4)}$$

Where M is mass of the analyte diffusing through an area (A) in a given time (t).

Combining equation ***Eq. S3*** and ***Eq. S4***, ***Eq. S5*** is obtained.

$$C = \frac{M\Delta g}{DAt} \quad \textbf{(S5)}$$

When DGT was deployed in the soils, it should be mentioned that $C_{DGT}$ not only include the soluble ions in porewater, but also consider the resupply from complexes and desorption from solid phase. The contribution of complexes and solid phase to $C_{DGT}$ mainly depends on the lability of the complexes and the absorbed fraction.

**Table S1.** Instrumental parameters for LA-ICP-MS analysis

| | Instrument condition | | Xiamen | Nanjing |
|---|---|---|---|---|
| ICPMS | Instrument | | Agilent 7700 | 1550W |
| | RF power | | 1400W | 0.8 L/min |
| | Ar flow rate | | 1.1 L/min | He |
| | Laser cell gas | | He | 0.5 L/min |
| | Carrier gas flow rate | | 0.7 L/min | Ni |
| | Cones | | Pt | Dual |
| | Detection mode | | Dual | TRA(time resolved analysis) |
| | Acquisition mode | | TRA(time resolved analysis) | TRA(time resolved analysis) |
| | Isotopes monitored | | $^{75}As$ $^{208}Pb$ $^{56}Fe$ | $^{13}C$ |
| | Internal standard | | $^{13}C$ | $^{13}C$ |
| Laser ablation | Instrument | | New Wave UP-213(Nd-YAG) | New Wave UP-213(Nd-YAG) |
| | Wavelength | | 213nm | 213nm |
| | Pulse length | | <4 ns | <4 ns |
| | Output energy | | 60% | 10% |
| | Ablation mode: line scan | Line width | 100 um | 100 um |
| | | Line length | 10 mm | 10 mm |
| | | Speed | 100 um $s^{-1}$ | 100 um $s^{-1}$ |
| | | Repetition rate | 20 Hz | 5 Hz |

All sample gels and gel standards for As and Pb were analyzed by LA-ICP-MS system in Xiamen while gel standards for Fe were analyzed by LA-ICP-MS system in Nanjing. 12 sample gels were reanalyzed for getting conversion factor between signal responses from two systems.

**Table S2** LOD, SD, and resolution of LA-ICP-MS analysis of gel standards

| | LOD (ng $cm^{-2}$) | SD (%) | Resolution (μm) |
|---|---|---|---|
| As(PF) | 0.83 | 8.5 | 164 |
| As(PZ) | 0.35 | 14.7 | 164 |
| Pb | 3.3 | 11.5 | 121 |
| Fe | 16 | 6.2 | 115 |

SD was calculated as average within a series of gel standards for each gel type

**Table S3** Change of Eh with depth in the studied field measured at the end of July, 2018

| Depth | 0~5 cm | 10~15 cm | 20~25 cm |
|---|---|---|---|
| Eh (mV) | -158±23 a | -156±34 a | -176±19 b |

a and b denote different statistical groupings ($p<0.05$).

**Table S4** Lateral variation of pH and total contents of As, Pb, and Fe in the studied field

| Sampling site | pH | As (mg/kg) | Pb (mg/kg) | Fe (mg/kg) |
|---|---|---|---|---|
| 1 | 7.16 | 8.63±0.65 | 40.5±0.66 | 34.7±1.6 |
| 2 | 7.12 | 8.22±0.37 | 39.5±1.94 | 36.4±0.5 |
| 3 | 6.96 | 8.51±0.19 | 36.9±1.95 | 37.4±0.2 |
| 4 | 5.81 | 7.02±0.17 | 39.6±1.91 | 35.9±0.9 |
| 5 | 5.72 | 7.42±0.42 | 40.0±1.53 | 35.3±0.4 |
| 6 | 5.41 | 7.55±0.28 | 41.6±1.84 | 35.5±0.7 |
| 7 | 5.49 | 7.76±0.45 | 42.1±1.57 | 35.9±1.5 |
| 8 | 5.77 | 7.38±0.68 | 43.1±3.29 | 36.1±0.6 |
| 9 | 5.74 | 7.18±0.15 | 42.5±2.19 | 35.3±0.5 |

There is no statistically significant difference ($p$=0.05) between different sub-sites within the paddy field.

**Table S5.** Vertical variation of total As, Pb and Fe concentrations, porosity and TOC in the studied field

| Depth (cm) | Total contents | | | porosity | TOC | pH |
|---|---|---|---|---|---|---|
| | As | Pb | Fe | | | |
| 0-5 | 6.97±0.94 a | 42.1±0.4 b | 31.3±0.5 a | 0.58 | 4.09±0.13 d | 5.54 |
| 5-10 | 6.99±0.47 a | 41.9±0.5 b | 31.9±0.4 a | 0.53 | 3.68±0.10 c | 5.38 |
| 10-15 | 7.21±0.45 a | 42.5±1.1 b | 32.0±1.3 a | 0.46 | 3.08±0.01 b | 5.79 |
| 15-20 | 6.03±0.71 a | 30.3±3.8 a | 29.3±3.1 a | 0.38 | 1.61±0.04 a | 6.65 |
| 20-25 | 6.27±0.35 a | 31.5±0.7 a | 32.7±0.7 a | 0.37 | 1.46±0.10 a | 6.80 |

a, b, c, d denote different statistical groupings ($p$<0.05).

**Table S6.** Analysis of Variance of sampling sites and vertical zones on CDGT of As, Pb, Fe, and $S^{(-II)}$.

| | Degrees freedom | Adjusted means square | *F* | *P* |
|---|---|---|---|---|
| **$C_{DGT}$ of As** | | | | |
| Sampling site (←→) | 8 | 1762 | 1.65 | >0.05 |
| Vertical zones (↑↓) | 2 | 94637 | 88.63 | <0.001 |
| Sampling site × Vertical zones | 16 | 1057 | 0.99 | >0.05 |
| **$C_{DGT}$ of Pb** | | | | |
| Sampling site) | 8 | 5924 | 3.34 | <0.001 |
| Vertical zones | 2 | 2700 | 1.52 | >0.05 |
| Sampling site × Vertical zones | 16 | 2842 | 1.60 | >0.05 |
| **$C_{DGT}$ of Fe** | | | | |
| Sampling site | 8 | 5864 | 5.56 | <0.001 |
| Vertical zones | 2 | 28482 | 26.99 | <0.001 |
| Sampling site × Vertical zones | 16 | 1974 | 1.87 | >0.05 |
| **$S^{(-II)}$ Gray-scale values** | | | | |
| Sampling site | 8 | 15965 | 9.14 | <0.001 |
| Vertical zones | 2 | 24568 | 14.07 | <0.001 |
| Sampling site × Vertical zones | 16 | 3362 | 1.93 | <0.05 |

**Table S7.** Pearson correlations among As, Pb, Fe fluxes, and $S^{(-II)}$ gray-scale value based on PADDI measurement

| | | DGT fluxes | | | $S^{(-II)}$ Gray-scale value |
|---|---|---|---|---|---|
| | | As | Pb | Fe | |
| DGT fluxes | As | 1 | -0.095 | 0.130 | -0.275** |
| | Pb | | 1 | 0.809** | -0.146** |
| | Fe | | | 1 | -0.296** |
| $S^{(-II)}$ Gray-scale value | | | | | 1 |

** means correlation is significant at the level of $p < 0.01$; * means correlation is significant at the level of $p < 0.05$.

**Table S8** High and low weather summary for the sample site

| | Temperature ($^{o}$C) | | Humidity (%) | | Pressure (mbar) | |
|---|---|---|---|---|---|---|
| | June | July | June | July | June | July |
| High | 35 | 39 | 100 | 100 | 1012 | 1013 |
| Low | 14 | 22 | 35 | 40 | 998 | 997 |
| Average | 24 | 29 | 85 | 81 | 1006 | 1005 |

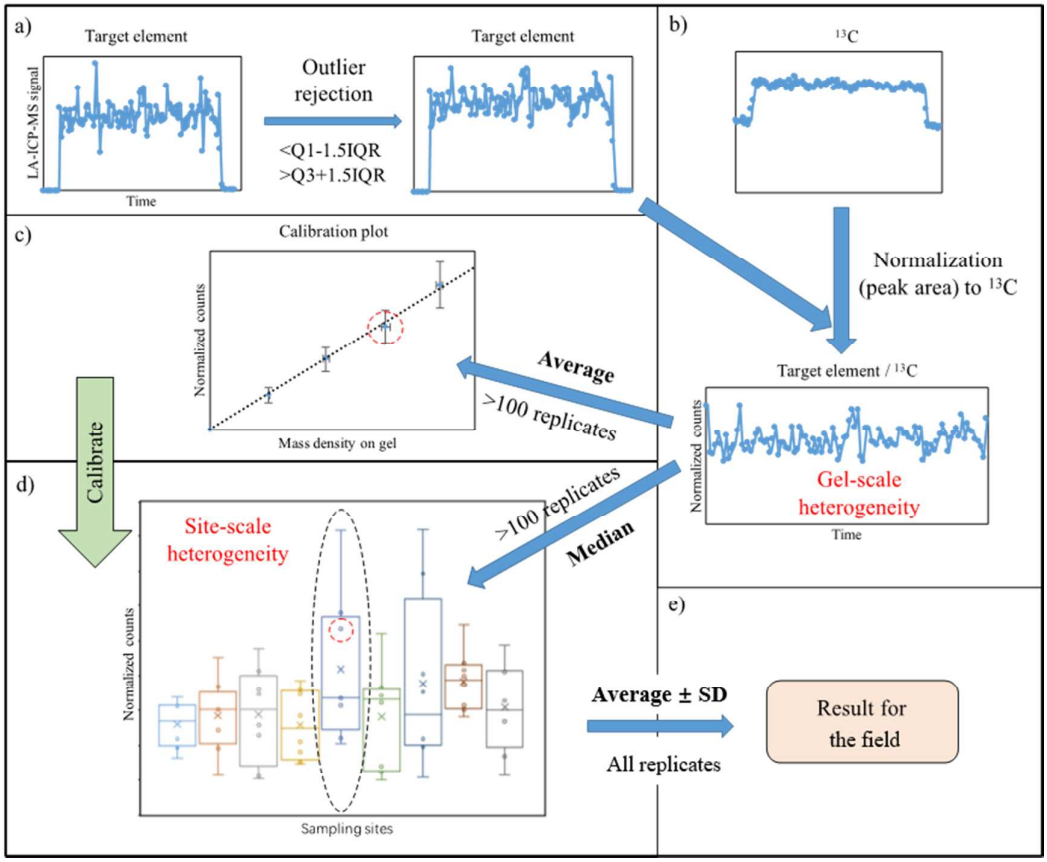


**Figure S2.** Data processing for standard and sample gels. a) outlier rejection; b) signal normalization to internal standard $^{13}C$; c) Calibrations derived from standard gels; d) Calculating mass loading of target elements on sample gels based on the medians of normalized counts; e) result for one paddy field (average ± standard deviation)

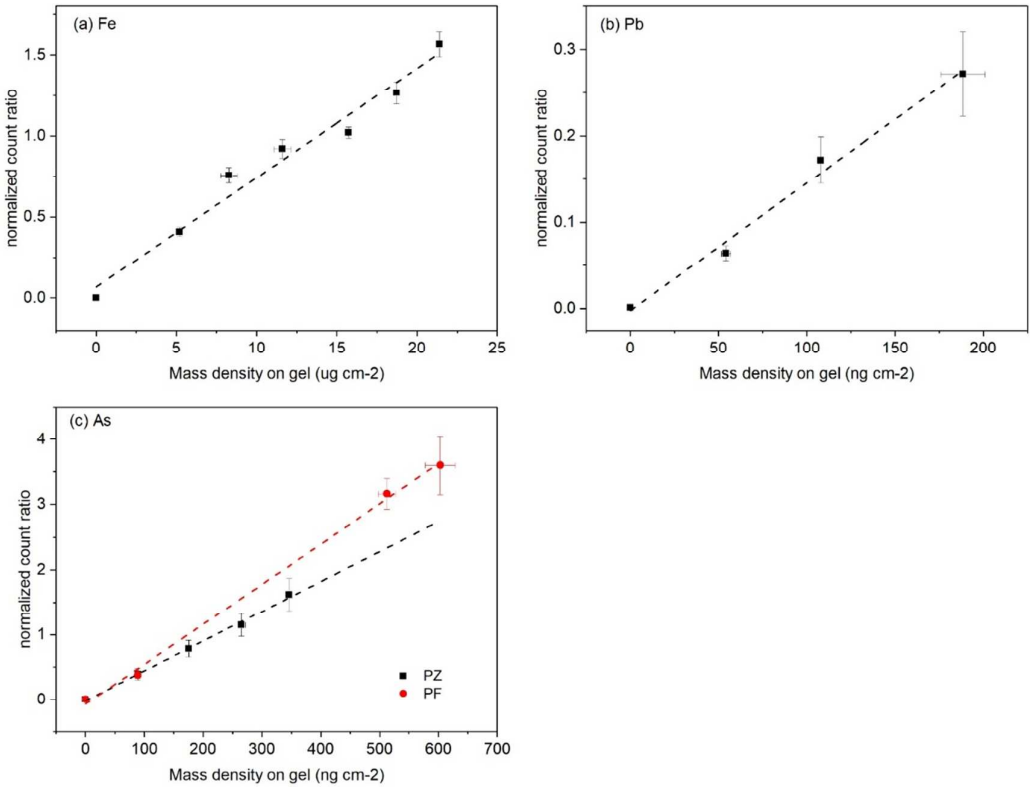


**Figure S3.** The relationship between mass loading on binding gels (ng $cm^{-2}$) and normalized metal count rate (metal count rate divided by $^{13}C$-count rate) quantitatively obtained through LA-ICP-MS analysis

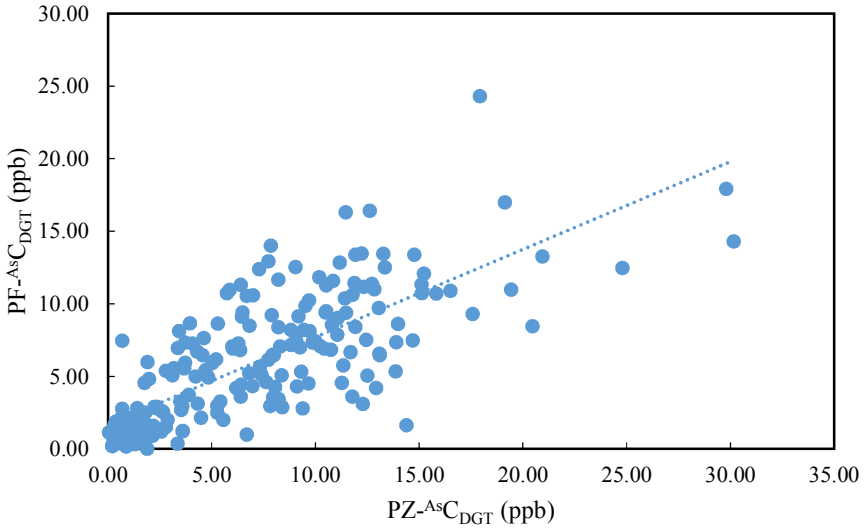


**Figure S4.** Relationship between $^{As}C_{DGT}$ measured by PZ-DGT and PF-DGT

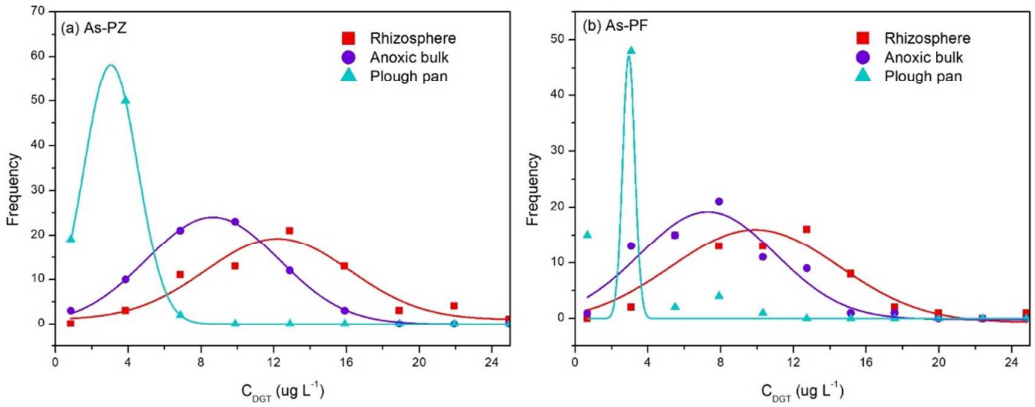


**Figure S5.** Frequency distributions of 72 replicates for $^{As}C_{DGT}$ measured by PZ and PF binding gels at the whole field scale.

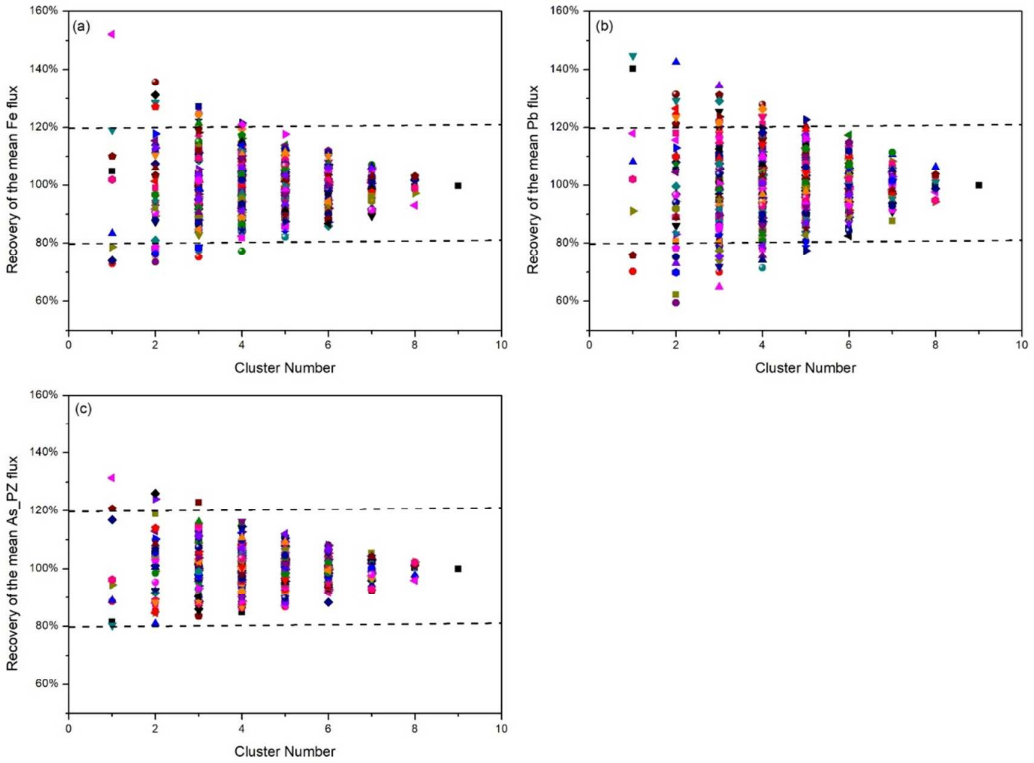


**Figure S6.** The change of recovery of the mean (a) $^{Fe}C_{DGT}$, (b) $^{Pb}C_{DGT}$, and (c) $^{As}C_{DGT}$ at the soil zonation of rhizosphere with different cluster sampling number.

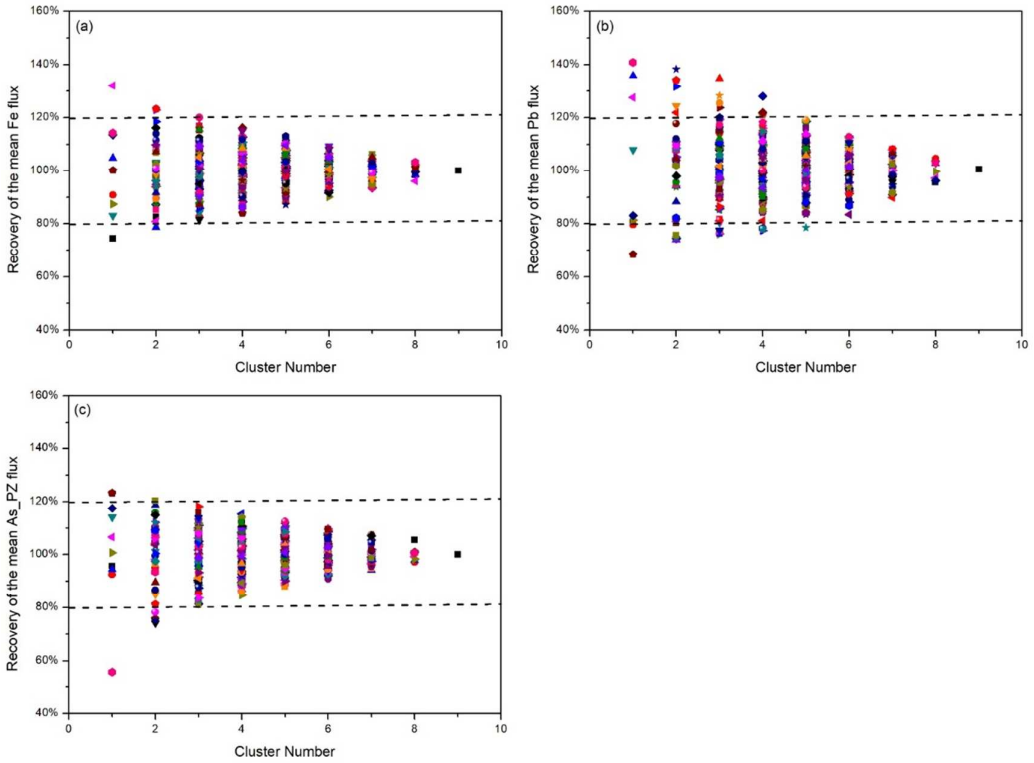


**Figure S7.** The change of recovery of the mean (a) $^{Fe}C_{DGT}$, (b) $^{Pb}C_{DGT}$, and (c) $^{As}C_{DGT}$ at the soil zonation of anoxic bulk with different cluster sampling number.

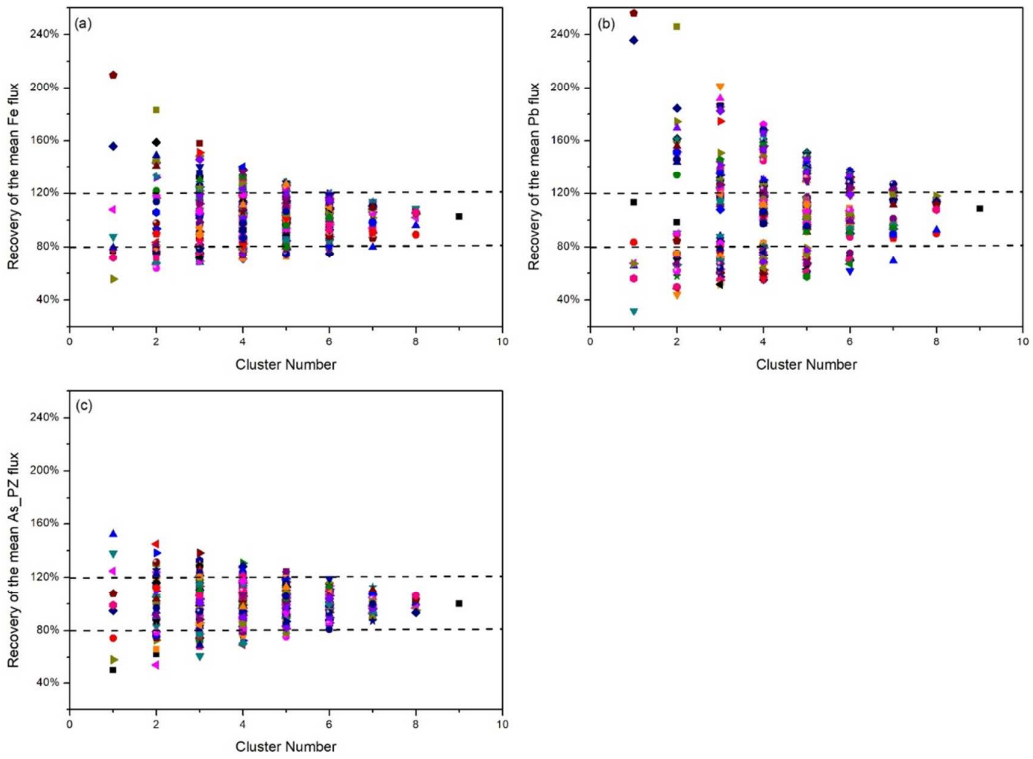


**Figure S8.** The change of recovery of the mean (a) $^{Fe}C_{DGT}$, (b) $^{Pb}C_{DGT}$, and (c) $^{As}C_{DGT}$ at the soil zonation of plough pan with different cluster sampling number.

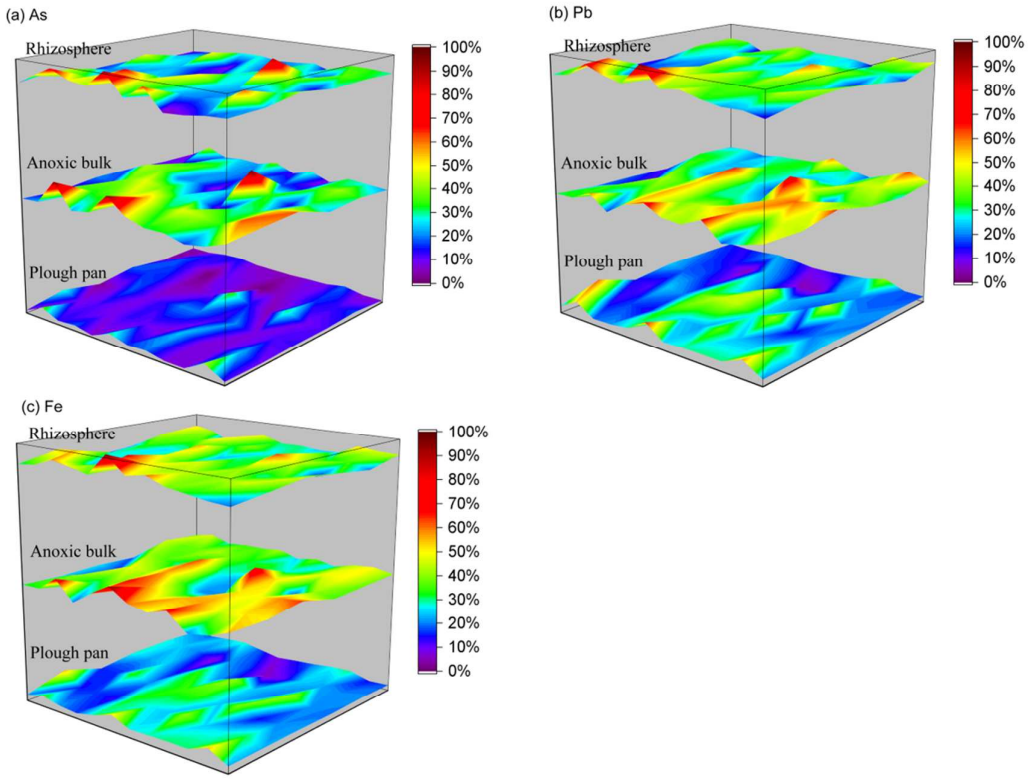


**Figure S9.** Field scale heterogeneity in relative porewater concentraions of As, Fe, and Pb.